Measurement of Tryptophan in Cell Cultures Using Fast Scan Cyclic Voltammetry at Carbon Fiber Microelectrodes with Improved Sensitivity and Selectivity

Isabella Schapira[1], Lily Russo-Savage[2], Terdha Narla[3], Maggie O'Neill[1], Kathryn A. Laprade[4], James M. Stafford[2,4], Yangguang Ou*[1,2]

[1] Department of Chemistry, University of Vermont, Burlington, VT 05405
[2] Neuroscience Graduate Program, University of Vermont, Burlington, VT 05405
[3] Department of Pharmacology, University of Vermont, Burlington, VT 05405
[4] Department of Neurological Sciences, University of Vermont, Burlington, VT 05405
* Corresponding author contact info: you@uvm.edu

Abstract

Establishing a sensitive and selective method to measure tryptophan *in situ* with good spatiotemporal resolution is invaluable to understanding its biological role and activity in nutrition, health, brain disorders, and the gut-brain axis. Here, we report on a sensitive and selective method to measure tryptophan over its main interfering species tyrosine. Specifically, we achieve this using fast scan cyclic voltammetry at carbon fiber microelectrodes via the application of an optimized multi-scan rate sawhorse waveform. We report over four-fold increase in sensitivity over previously reported methods and a six-fold selectivity of tryptophan quantitation over that of tyrosine. We demonstrate the utility of our method via measuring extracellular Trp in cultured PC-12 cells and PC-12 cells with overexpressed tryptophan hydroxylase 2.

Introduction

Tryptophan (Trp) is one of the 20 naturally occurring amino acids that play a fundamental role in nutrition and health[1]. It is also the precursor to several brain neurotransmitters (i.e. serotonin, melatonin)[1] and biomarkers that participate in the crosstalk in the gut-brain axis (i.e. kynurenine, vitamin B_6)[2, 3]. As a result, it has been hypothesized that Trp itself plays crucial roles in the brain, the gut, and the various disorders that involve the gut-brain axis, including autism spectrum disorder (ASD)[4] and depression[5].

One of the most common techniques for Trp monitoring in foods, body fluids, and tissue is chromatography. However, chromatography is plagued by issues of Trp degradation due to acid hydrolysis treatment of proteins. To combat this issue, researchers have come up with acid derivatization methods[6-9] and better protection groups[10, 11]. For free Trp measurements, researchers often rely on colorimetric methods, near-infrared reflectance spectroscopy, optimized high performance liquid chromatography with mass spectrometry detection, and isotopic labelling (reviewed in Friedman[1]).

While these are powerful methods that have provided a plethora of valuable information, these methods are either offline (meaning *ex situ*), require a specialist to operate the instrumentation, necessitate the removal of interfering signals from other aromatic amino acids such as tyrosine (Tyr), and/or involve sample treatment protocols before the analytes can be quantified. Thus, there is still a need for a sensitive and selective Trp quantitation technique for *in situ* monitoring in cells, tissues, and *in vivo*. Moreover, release dynamics of Trp metabolites in the brain occur on the order of subseconds[12, 13], so it is possible Trp dynamics occurs on comparable scales as well. Furthermore, Trp concentrations are hypothesized to vary between different cell types and brain regions[14, 15] so micron-scale spatial resolution would be advantageous. One of the techniques capable of making measurements at the appropriate spatiotemporal scale is fast scan cyclic voltammetry (FSCV) at carbon fiber microelectrodes (CFMs). The Ross lab demonstrated the utility of FSCV at CFMs (via the application of the dopamine waveform) to measure electroactive amino acids, including Trp, with 100 ms timescale and micron spatial resolution[16]. However, their paper did not

demonstrate selective measurement of Trp over dominant interfering species such as Tyr, which has overlapping oxidation peaks.

In this work, we utilize a sawhorse waveform and optimize its parameters to gain significant selectivity of Trp detection over that for Tyr. In fact, we demonstrate that our optimized conditions permit high selectivity for Trp detection over that for Tyr while maintaining high sensitivity for Trp. We also demonstrate the utility of our method in a real sample by measuring exogenous Trp in cultured PC-12 cells.

Experimental Section

Chemicals and Instrumentation

The chemicals used were analytical grade and were purchased from MilliporeSigma (St. Louis, MO). Phosphate buffered saline (PBS) tablets were purchased from Fisher Bioreagents (Waltham, MA, USA). 1x PBS (pH 7.40) was prepared by dissolving five PBS tablets in 1.0 L nanopure water (Milli-Q IQ7000, MilliporeSigma, St. Louis, MO). 0.5 mM Trp and Tyr stock solutions were prepared in PBS and frozen into small aliquots until use. On the day of the experiment, stock solutions were thawed at room temperature and standard solutions of 0.5 µM, 1 µM, 3 µM, and 5 µM tryptophan and tyrosine solutions were prepared from the stock.

Electrode Fabrication and Fast Scan Cyclic Voltammetry

A single carbon fiber (GoodFellow, Pittsburgh, PA, USA) of 7 µm diameter was aspirated into a 0.5 mm inner diameter (1.00 mm outer) borosilicate glass capillary (A-M Systems, Inc., Carlsberg, WA, USA) using a vacuum pump (Gast). These filled capillary tubes were subsequently pulled using a vertical puller (PC-100 or PE-22, Narishige Group, Japan) to create a tapered seal insulating the carbon fiber. While observing the electrode under a microscope, the protruding carbon fiber was then cut to a length between 130 µm to 160 µm. All the results below are reported as current densities, in which the measured current is normalized to the geometric surface area of the electrode and reported in unit of $pA/\mu m^2$. A nichrome wire with a soldered pin (Phoenix Enterprises/PE Connectors, Chatsworth, CA, USA) was then coated with silver epoxy paint (GC Electronics, Rockford, IL, USA) and inserted into the distal end of the fiber-filled capillary. A polyolefin heat shrink tubing (Mouser, Mansfield, TX, USA) then is heat-sealed around the electrode/nichrome wire junction to secure them in place.

We employed a 2-electrode system comprised of a pseudo-Ag/AgCl reference (made in-house) and the CFM working electrode. Fast scan cyclic voltammetry (FSCV) was performed using a custom-built integration unit that includes a Dagan Chem-Clamp (Dagan Corporation, Minneapolis, MN, USA), National Instrument data acquisition cards, Pine Instrument Dagan-compatible headstage, and WCCV 3.6 software (Knowmad Technologies LLC, Tucson, AZ, USA). All experiments were performed in a Faraday cage (AutoMate, Berkeley, CA, USA). Electrodes were cycled in each solution for 10 min prior to any data acquisition. A sawhorse waveform was applied at a frequency of 10 Hz for all experiments. More details on the waveform are presented later in Results and Discussion.

Flow injection analysis (FIA)

A continuous flow of PBS (buffer) was pumped into a flow cell (built in-house, Cole-Parmer, Vernon Hills, IL) at 1.81 mL/min using a syringe pump (Fisher Scientific, Waltham, MA, USA). Reference and working electrodes were attached to the flow cell accordingly. A 5-s bolus of Trp, Tyr, or both was introduced to the electrodes by using a 6-port injection valve (VICI, Houston, TX, USA).

Data collection

Custom software WCCV 3.6 software (Knowmad Technologies LLC, Tucson, AZ, USA) was employed for the collection and analysis of data, which includes background subtraction, signal averaging, and digital filtering. Data was filtered using a fourth order Butterworth low pass filter. The cyclic voltammograms (CVs) and i-t (current vs time) plots were stacked over time to create a 2D color plot. The x-axis is time (30 s files unless otherwise stated), the y-axis is potential applied (V), and the color indicates current. The CVs and i-t plots were exported as text files and analyzed in Excel and GraphPad Prism 9. The max currents at the oxidation peak corresponding to Trp oxidation (~1.0 V vs. pseudo Ag/AgCl) were normalized to the geometric surface area of each electrode. Grubbs test was used to remove any outliers and errors were propagated appropriately to combine the different trials from different electrodes. All statistical tests, including Grubbs', t-tests, and one-way ANOVA Dunnett T3 multiple comparison test, were conducted in GraphPad Prism 9.

Cell culture

PC-12 cells (CRL-1721.1, ATCC, Manassas, VA, USA) were cultured in RPMI-1640 media (A10491, Gibco, Jenks, OK, USA) containing 10% horse serum, 5% fetal bovine serum and 5% penicillin streptomycin (30-002-Cl, Corning, Corning, NY, USA). Media was changed every 2-3 days and cells were passaged at ~80% confluency by dissociating with trypsin. Cells were maintained on standard treated tissue culture dishes in a 37ºC humidified incubator with 5% CO_2 until FSCV measurements were ready to be performed. For FSCV recordings, cells were removed from the incubator and transported to the Faraday cages. Manual micromanipulators (Narashige Group, Japan) were used to submerge the CFMs into the media and approach the cells as close as possible without breaking. We then measured ~2-3 seconds of FSCV background before using a micropipette to exogenously apply 5 μM Trp into the media near the CFM while continuously recording for up to 60 seconds. This was repeated 4 more times at different locations in the well plate as well as in different culture plates for PC-12 cells. We performed these measurements 6 times for PC-12 cells with overexpression of TPH2.

Generation of TPH2 overexpressing PC-12

TPH2 cDNA was subcloned from vector MHS6278 (Horizon Discovery Biosciences) into the pLVX-EF1α-IRES-mCherry vector (Clontech 631987) to drive expression of TPH2 using the EF1α promoter (pLVX-EF1α-TPH2-IRES-mCherry). Lentivirus was packaged using a standard lentiviral packaging protocol. Briefly, 9 μg total of lentiviral vectors were transduced into a 10cM plate of 80% HEK293FT cells comprising 5 μg of pLVX-EF1α-TPH2-IRES-mCherry, 3.75 μg of psPAX, and 1.25 μg of pMD2.G. Media was change 24 hours later with viral supernatant harvested 48 hours later. Viral supernatant was used to infect PC-12 cells, which were later sorted by fluorescence-activated cell sorting (FACS) for mCherry. Over expression of TPH2 was validated by standard western blot procedure (Figure 1) followed by chemiluminescent imaging[17]. Antibodies used were TPH2 (Abcam ab111828) and GAPDH (Proteintech 60004) primary antibodies.

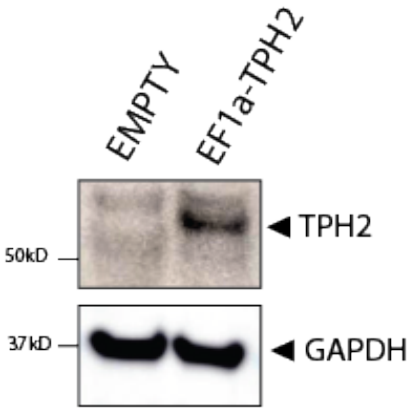

Figure 1. Validation of TPH2 overexpressing PC-12 cells. Western blot for TPH2 shows strong overexpression of TPH2 (predicted molecular weight ~56kD) in the pLVX-EF1α-TPH2-IRES-mCherry expressing cell line relative to cells expressing an empty vector. GAPDH loading control is shown as reference.

Results and Discussion

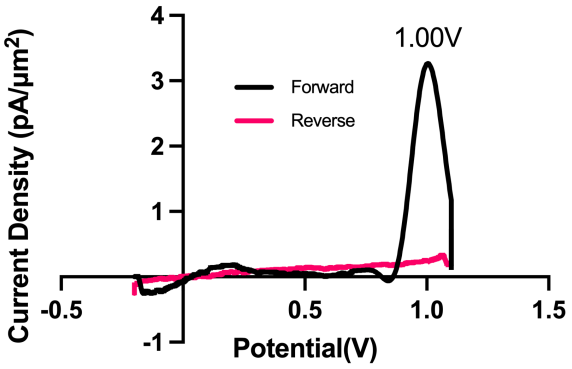

Figure 2. Representative cyclic voltammogram for Trp oxidation on carbon fiber microelectrode using the multi-scan rate waveform. Black trace indicates the forward scan while the red trace indicates the reverse scan. The primary oxidation peak occurs at 1.00 V.

Trp is one of the 20 naturally occurring aromatic amino acids and is electroactive, meaning it can be readily oxidized or reduced. Nguyen et al.[18] demonstrated that Trp undergoes an initial 2-electron, 2-proton oxidation, a step that was attributed to the largest observed anodic peak at 0.9 V on a pyrolytic graphite electrode vs. SCE. Others[19] have attributed the loss of the pyrrolic double bond and addition of a ketone adjacent to the secondary amine as the primary oxidation event observed on glassy carbon (vs. Ag/AgCl (3M KCl)). Trp oxidation was observed using FSCV at CFM by Ross and colleagues[16] at 1.06 V, and we observe a similar oxidation peak at 1.0 V on the forward scan (Figure 2).

The waveform parameters (holding potential, transition potential, switching potential, switching potential duration, and scan rate) of a multi-scan rate sawhorse waveform (MSW) were optimized for the sensitive and selective detection of Trp over Tyr. The original MSW (Figure 3a) was derived from work published by Sombers and colleagues for the detection of enkephalin using FSCV at CFMs[20, 21]. The first scan rate between the holding potential (A, Figure 3a) and transition potential (B, Figure 3a) was held constant at 100 V/s because there are no oxidation or reduction peaks of interest occurring in those potentials. The primary oxidation peak occurs between the transition potential (B, Figure 3a) and the switching potential (C, Figure 3a). The scan rate in this potential range was varied (discussed below).

Each parameter in the MSW (*vide supra*) was varied systematically. The assumption is that these parameters behave independently from each other, and, from our experience, there has been no evidence indicating otherwise. Figure 3b-3f summarizes the results from the optimization of MSW waveform parameters for maximal sensitivity towards Trp detection. Maximum sensitivity towards Trp detection was observed at intermediate values that we tested for the holding potential, transition potential, and switching potentials. The utility of the holding potential is to: 1) oxidize interfering species such that their anodic currents become part of the background signal (and can be subtracted out); and/or 2) preconcentrate analytes of interest through electrostatic interactions. A -0.3 V holding potential yielded the maximal sensitivity, which makes sense as at pH 7.40, the majority of the Trp molecules have the positive charge on the amino terminal group, so a negative surface potential on the electrode would preconcentrate it onto the electrode surface. It is possible that scanning the holding potential to even more negative values would preconcentrate interfering species, thereby lowering the sensitivity for Trp. The optimal transition potential was +0.6 V and the optimal switching potential was +1.2 V. The transition potential is the point where the scan rate switches from 100 V/s to higher scan rates and should precede the potential at which we expect our primary oxidation peak. At potentials between the holding and transition potential, the signals were suppressed due to the slower scan rate (i.e. 100 V/s). Thus, the smaller oxidation peak in Trp (~0.43 V in Weese-Myers et al.[16]) is no longer apparent here. The switching potential is the upper limit potential and serves to: 1) over-oxidize the surface groups to increase adsorption; and/or 2) renew the electrode surface by stripping the topmost layer of carbon. These phenomena have been observed and discussed by others prior[21-23].

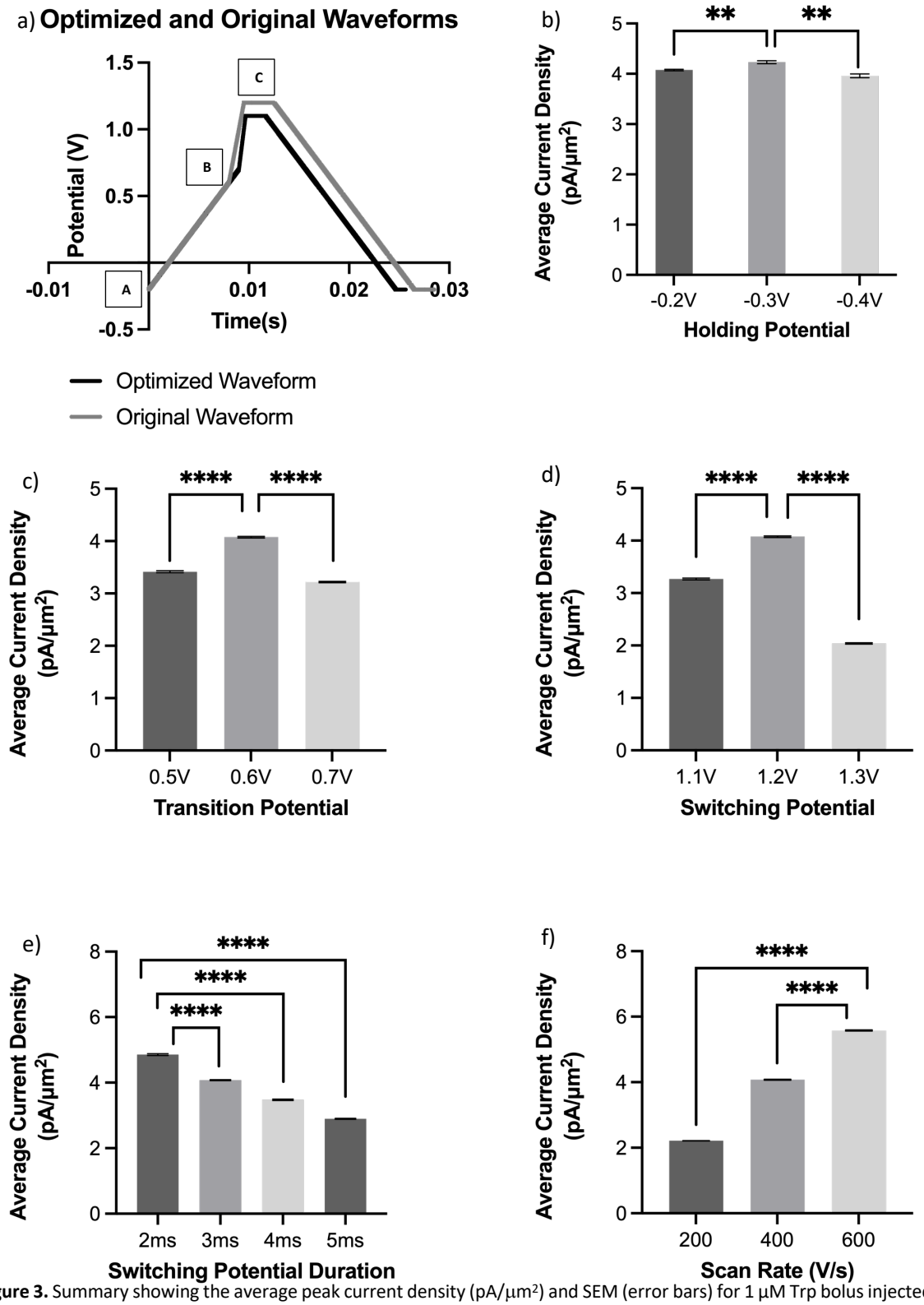

Figure 3. Summary showing the average peak current density (pA/µm²) and SEM (error bars) for 1 µM Trp bolus injected into the flow injection analysis system for each respective parameter. The average current densities were calculated by averaging the points in the bolus region of the IT curves for each electrode and then averaging these values together between electrodes (and propagating the appropriate SEMs). a) is an overlay of the original and optimized waveforms. Point A indicates holding potential, B is the transition potential, and C is the switching potential. b) Current density was greatest for a holding potential of -0.3V over those at -0.2V and -0.4V. c) The largest signal for Trp was found to be with a transition potential of +0.6V over those of +0.5V and +0.7V. d) The average current density was highest for switching potential of +1.2V when compared to those at +1.1V and +1.3V. e) The switching potential duration of 2 ms yielded the largest average current density when compared to longer hold times (3, 4, or 5 ms). f) The scan rate that yielded the largest signal was 600V/s when compared to 200V/s and 400V/s. **p <0.01, ****p<0.0001.

Maximal sensitivity for Trp was observed when the switching potential (or amperometric potential as referred to by Calhoun et al.[20]) was held for 2 ms (Figure 3e). Longer duration displays a scenario of diminishing returns. We hypothesize that longer holding time at the switching or amperometric potential could chemically alter the functional groups such that they are less favorable for Trp and/or more favorable for its interfering species. Lastly, the maximal sensitivity was observed for the 600 V/s scan rate over the lower values (Figure 3f). This makes sense as there is an expected increase in signal over background with an increase in scan rate, in agreement with those reported previously[24]. There is a limit, however, as too high of a scan rate would outrun electron transfer kinetics.

We then assessed how the different waveform parameters above can be utilized to optimize for selectivity of Trp over Tyr signal. This is of particular interest as Trp and Tyr has a maximum oxidation peak at the same potential (~1.0 V) in an FSCV experiment on a CFM vs. Ag/AgCl. We injected boluses of 1 μM Trp and, separately, boluses of 1 μM Tyr into the FIA system and evaluated their respective current densities at 1.0 V vs. Ag/AgCl. Unless otherwise stated we tested 3-5 electrodes per condition. Then the current density from Trp oxidation peak was divided by that for the Tyr oxidation peak from the same conditions to yield a Trp:Tyr selectivity ratio. We observed that a holding potential of -0.2 V yielded the highest selectivity ratio for Trp:Tyr (Figure 4a). Now this optimal condition for selectivity differed from that for optimal holding potential for sensitivity (*vide supra*). Because the loss in selectivity (-50%) going from -0.2 V to -0.3 V holding potential was significantly greater than the gain in sensitivity going from -0.2 V to -0.3 V (+3.8%), we decided to select -0.2 V as the optimal holding potential overall. Moreover, we observed that a transition potential of +0.7 V yielded the highest selectivity ratio compared to those of smaller values (Figure 4b). The optimal transition potential for sensitivity was determined to be +0.6 V (see above). The loss in selectivity (-87%) was significantly greater going from +0.7 to +0.6 V than the gain in sensitivity from +0.7 to +0.6 V (+27%). Thus, the optimal transition potential we selected was +0.7 V. For switching potential, we discovered that a switching potential of +1.1 V yielded the highest selectivity ratio (Figure 4c). This contrasted with the +1.2 V switching potential determined to yield the maximum sensitivity. Here, the relative loss of selectivity/gain of sensitivity were relatively comparable (~20-25%) so we opted to go with +1.1 V in favor of slightly higher selectivity for a slight loss in sensitivity. For switching potential duration, 2 ms was the optimal condition that yielded the maximum sensitivity and selectivity (Figure 4d). Likewise, the highest scan rate we tested (600 V/s) yielded the highest sensitivity (*vide supra*) and highest selectivity for Trp over Tyr (Figure 4e).

We have demonstrated above a significant improvement in selectivity for Trp oxidation over that for Tyr with the optimized MSW (Figure 3a, -0.2 V holding, +0.7 V transition, +1.1 V switching, 2 ms duration of switching potential, 600 V/s scan rate between the transition and switching potentials). We then wanted to assess whether the presence of Tyr in the same solution would affect the Trp signal in any way. Thus, we performed injections of a mixture of 1 μM Trp + 1 μM Tyr into the FIA and compared/contrasted that current density with those of Trp and Tyr alone (Figure 4f). We observed that while there is a significant drop in Trp current density as a result of the presence of an equivalence concentration of Tyr, the current density is still significantly higher (4-fold) than that for Tyr alone. We hypothesize that this decrease is not due to the oxidation of Tyr at the electrode surface (since it's relatively small) but merely the shielding of Trp from interacting with the electrode by the presence of Tyr.

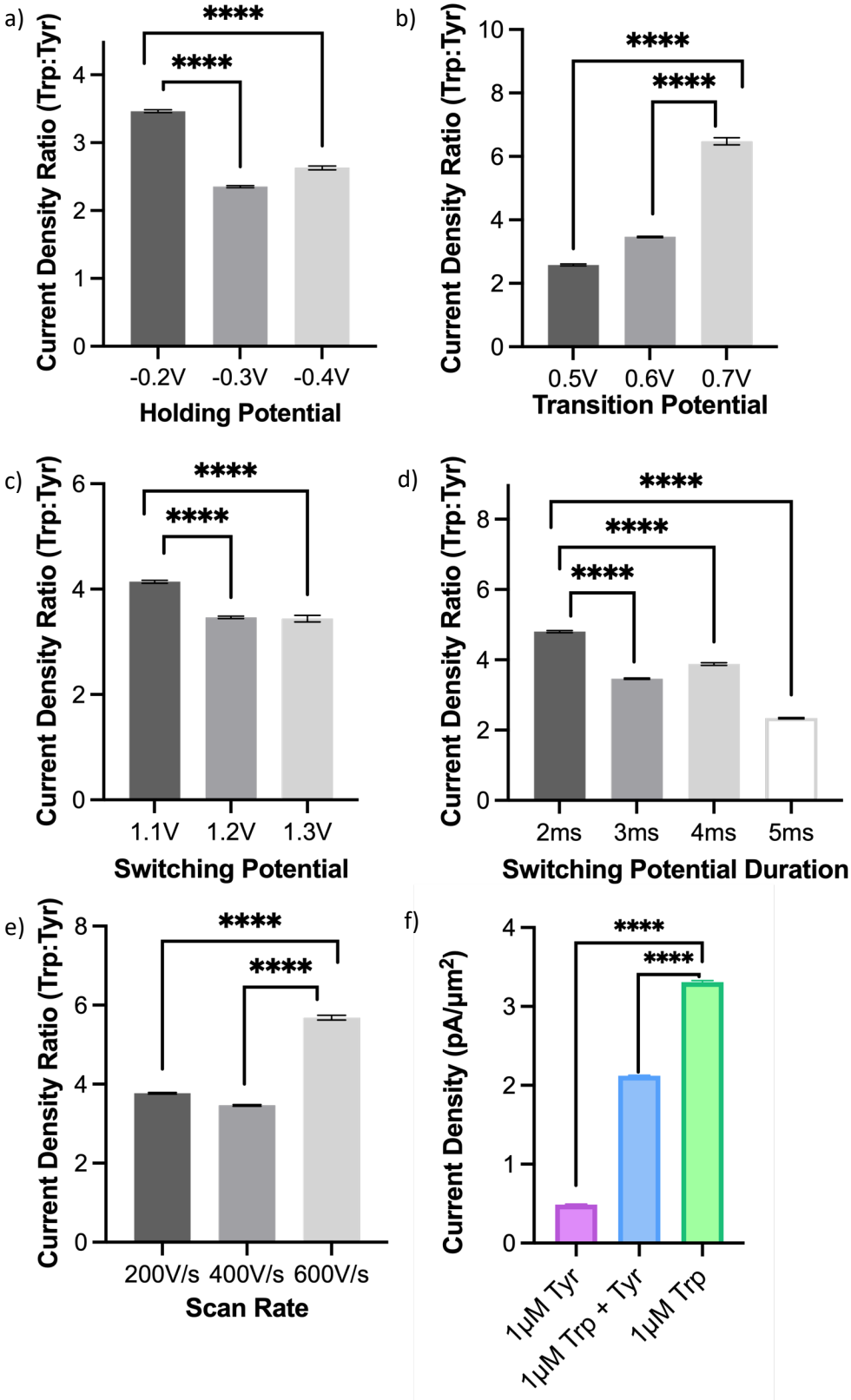

Figure 4. Plot of current densities of Trp to Tyr as an indicator of selectivity for the different optimized parameters: a) holding potential, b) transition potential, c) switching potential, d) duration of switching potential, and e) scan rate. f) Plot of current densities for individually injected Trp and Tyr solutions compared to that of a mixture of equivalent concentrations (1 µM) of both. Error bars are ± SEM. ****p<0.0001.

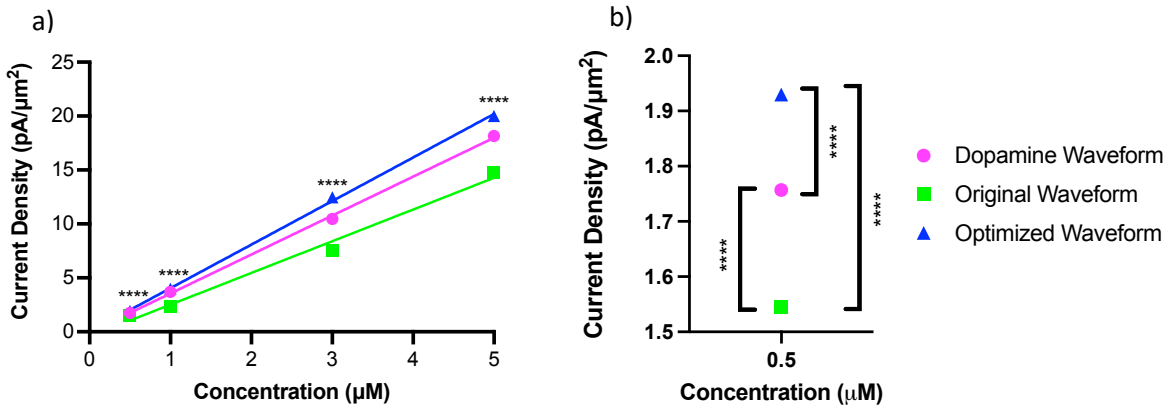

Figure 5. a) Calibration curves for Trp using three different waveforms (optimized MSW (green triangle), dopamine (magenta circle), and original MSW (blue square)). Error bars (±SEM) are too small to be visible. Only the t-test results comparing optimized vs. original waveforms are denoted in the graph. b) Zoomed-in plot of the 0.5 μM Trp showing how the optimized MSWs yielded higher current density than the dopamine and original waveform. ****p<0.0001.

As summarized in Figure 5a and 5b, the original MSW did yield significantly lower current density than the dopamine waveform at all concentrations (****p < 0.0001). The optimized MSW, however, yielded significantly higher sensitivity for Trp detection than the original MSW at all four concentrations that were evaluated (****p<0.0001). The optimized MSW yielded higher current density for Trp than the dopamine waveform at all concentrations evaluated (****p<0.0001).

Table 1. Summary of limit of detection (LOD) and limit of quantitation (LOQ) in nM for each of the three waveforms used for Trp measurements.

	Dopamine waveform	Original MSW	Optimized MSW
LOD (nM)	41 ± 20	190 ± 150	9.0 ± 0.6
LOQ (nM)	100 ± 30	290 ± 190	34 ± 6

These conclusions were further validated by the calculated limit of detection (LOD) and quantitation (LOQ) (Table 1). LOD and LOQ were calculated from standard deviation of the baseline noise in the IT curves and the corresponding calibration curve for each waveform (n = 5 for each category). There is no statistical difference between those reported for the dopamine and original MSW ($p = 0.0588$). Measurements using the optimized MSW, however, did show significantly lower LOD and LOQ than those for the dopamine ($p < 0.01$) and original MSW ($p < 0.05$). We conclude, therefore, that the optimized MSW provided conditions for the most sensitive detection of Trp of the three waveforms. In fact, based on these data, we can report a 4-fold improvement in the limit of detection using the optimized waveform compared to the dopamine waveform and a 20-fold better sensitivity compared to the original MSW.

Next, we investigated fouling on the electrode surface as a function of multiple repeated injections of Trp using the optimized waveform (Figure 6a). A one-way ANOVA Dunnett's T3 multiple comparison test revealed that there is no statistical difference between any of the 25 consecutive injections. When we

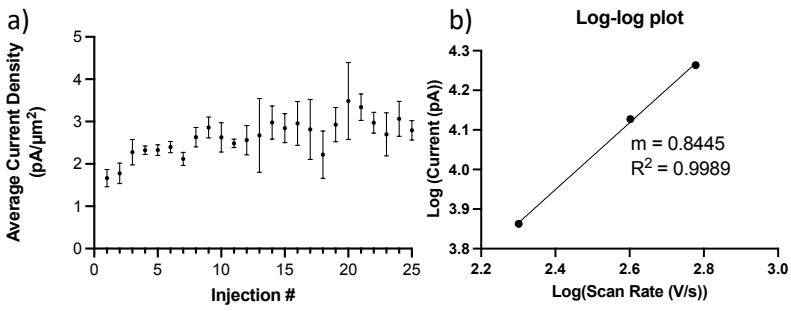

Figure 6. a) Average current density over 25 consecutive injections (error bars = SEM). b) Log-log plot of the current vs. scan rate showing that the slope is 0.8445.

binned the data into groups of 5 and performed the one-way ANOVA again, there was only statistical difference between the first five (1-5) injections and the last five (21-25) injections ($p = 0.0005$). Thus, we conclude that with the optimized waveform, multiple consecutive injections of at least 20 should not cause any fouling on the electrode surface. We hypothesize that >20 consecutive injections are still possible if cycling is performed in between to regenerate the electrode surfaces. We also obtained a slope of 0.8445 ± 0.0016 in a log-log plot of the current vs. scan rate (Figure 6b). Theory predicts that a slope of 1 is indicative of an entirely adsorption-driven process while a slope of 0.5 indicates a solely diffusion-driven process[7, 25, 26]. Our slope indicates that the signal we obtained is primarily adsorption-driven with some contribution from diffusion and this is in agreement with those reported by others[16, 26].

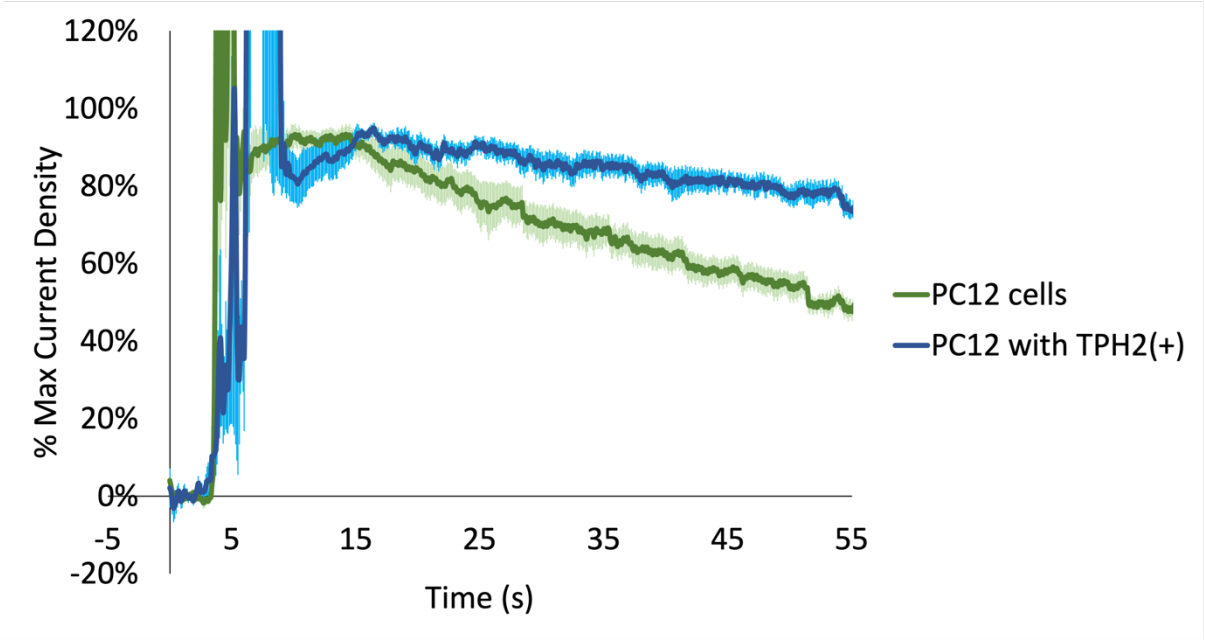

Figure 7. Normalized current density (to the maximum current in each curve, excluding those signals called by mechanical noise from the injection itself) for exogenously applied 10 ?L of 5 ?M Trp (red triangle) to cultured PC-12 cells (green, n = 5 measurements) and PC-12 cells with overexpressed tryptophan hydroxylase 2 (TPH2(+), n = 6 measurements). Pale blue and pale green error bars indicate SEM. ****p<0.0001.

Lastly, we performed Trp measurements in cultured PC-12 cells. While we may be the first to use FSCV at CFMs to measure Trp in cell cultures, we are not the first to use FSCV to measure Trp-containing compounds in cell cultures. In fact, Kennedy and colleagues utilized FSCV at CFMs to measure α-melanocyte stimulating hormone and other Trp- and Tyr-containing oligopeptides[26]. The authors reported comparable temporal resolution as our method reported here but utilized a slightly larger fiber (9 μm in diameter) beveled at 45^{o} into a disc electrode. Assuming an elliptical shape of the electrode, this would translate to a current density of ~4 pA/μm^2 for the authors' highest observed Trp or Trp-containing peptide. In contrast, with our method, we observe a nearly 2-fold higher current density under comparable conditions. Moreover, we perform further optimization for selectivity here.

We cultured two types of cells: PC12 and PC12 with an overexpression of tryptophan hydroxylase 2 (TPH2). TPH is the rate limiting enzyme in the synthesis of serotonin from Trp. While TPH1 is expressed primarily in the pineal gland and the periphery, TPH2 is expressed mainly in serotonergic neurons in the brain[27, 28]. We positioned a CFM in the extracellular media surrounding the cells (with a pseudo-Ag/AgCl in the same well as a reference electrode). We observed a large range of maximum current densities in the individual recordings even within the same well plate of cells. This can be rationalized by the fact that the current densities depend on: 1) how close the CFMs are positioned near the cell

membranes; and 2) how close the Trp is applied near the CFMs. In order to quantitatively compare between the different recordings, we normalized each current density vs. time profile to the maximum signal from the exogenously added Trp (excluding higher currents that were due to mechanical noise of adding the Trp itself, usually present at the time of addition). As seen in Figure 7, the normalized data revealed two distinct profiles. The general shape of the time profiles is similar for both types of PC-12 cells: there is an initial increase due to the application of the exogenous Trp and then a subsequent decay. Both decay curves should include contribution from mass transport (i.e. diffusion) and possibly from the activity of any membrane-bound transporters. We hypothesized that PC-12 cells with TPH2(+) have higher transporter activity to accommodate the higher expression of intracellular TPH2 and activity. However, that appeared to not be the case. Our data shows a slower decay curve for those Trp measurements done with PC-12 cells with TPH2(+) than their wildtype counterpart. Assuming that the Trp decay curves in both should experience similar contributions from mass transport, then the discrepancy between the two could indicate differences in transport activity that internalize amino acids such as Trp into the cells. In fact, these data are incredibly reproducible, as indicated by the relatively small error bars (±SEM) at each time point (pale blue for PC-12 with TPH2(+), pale green for PC-12 wildtype). Wilcoxon t-test results revealed a significant difference between the two decay profiles (****$p<0.0001$). A speculative hypothesis to explain these data is that the PC-12 cells with TPH2(+) may have lower expression of amino acid transporters[29, 30]. More experiments will be needed to evaluate and test this hypothesis. Nevertheless, these cell measurements demonstrate the utility of our optimized method for *in situ* Trp sensing in biological samples with good spatiotemporal resolution.

Conclusions

We developed an improved method for sensitive and selective Trp sensing via the application of an optimized multi-scan rate sawhorse waveform using FSCV at CFMs. We demonstrated four-fold higher sensitivity for Trp sensing over previous methods and a six-fold higher current density for Trp signals than those for Tyr, one of the primary interfering species that has similar oxidation potentials. We utilized the optimized method and measured exogenously applied extracellular Trp in two different cell lines: PC-12 and PC-12 with overexpression of TPH2. The time-dependent measurements revealed similar release, but interesting differences in the decay curves. While we demonstrated here the utility of the optimized waveform for sensitive and selective Trp detection over Tyr, further optimization may be necessary to reduce signals from other interfering species in complex matrices such as the brain and the gut.

Acknowledgements

TPH2 overexpressing cell line creation was supported under Defense Advanced Research Projects Agency (DARPA) agreement number FA8650-21-2-7120. This material is based on research sponsored by 711 Human Performance Wing (HPW) and DARPA under agreement number FA8650-21-2-7120. The U.S. Government is authorized to reproduce and distribute reprints for Governmental purposes notwithstanding any copyright notation thereon. The views and conclusions contained herein are those of the authors and should not be interpreted as necessarily representing the official policies or endorsements, either expressed or implied, of 711 HPW and DARPA or the U.S. Government.

The authors would also like to thank the University of Vermont for funding this work (YO, IS, LRS, TN, MO) and Dr. David Punihaole for useful discussions and editing of this manuscript.

Conflict of Interest

The authors have no conflict to report.

References

(1) Friedman, M. Analysis, nutrition, and health benefits of tryptophan. *International Journal of Tryptophan Research* **2018**, *11*, 1178646918802282.
(2) Kennedy, P. J.; Cryan, J. F.; Dinan, T. G.; Clarke, G. Kynurenine pathway metabolism and the microbiota-gut-brain axis. *Neuropharmacology* **2017**, *112*, 399-412.
(3) Li, Y.; Luo, Z.-Y.; Hu, Y.-Y.; Bi, Y.-W.; Yang, J.-M.; Zou, W.-J.; Song, Y.-L.; Li, S.; Shen, T.; Li, S.-J. The gut microbiota regulates autism-like behavior by mediating vitamin B6 homeostasis in EphB6-deficient mice. *Microbiome* **2020**, *8* (1), 1-23.
(4) Boccuto, L.; Chen, C.-F.; Pittman, A. R.; Skinner, C. D.; McCartney, H. J.; Jones, K.; Bochner, B. R.; Stevenson, R. E.; Schwartz, C. E. Decreased tryptophan metabolism in patients with autism spectrum disorders. *Molecular autism* **2013**, *4* (1), 1-10.
(5) Dell'Osso, L.; Carmassi, C.; Mucci, F.; Marazziti, D. Depression, serotonin and tryptophan. *Current pharmaceutical design* **2016**, *22* (8), 949-954.
(6) Gaitonde, M. K.; Dovey, T. A rapid and direct method for the quantitative determination of tryptophan in the intact protein. *Biochemical Journal* **1970**, *117* (5), 907-911.
(7) Zahnley, J. C.; Davis, J. G. Effect of high tyrosine content on the determination of tryptophan in protein by the acidic ninhydrin method. Application to chicken ovoinhibitor. *Biochemical Journal* **1973**, *135* (1), 59-61.
(8) Friedman, M. Applications of the ninhydrin reaction for analysis of amino acids, peptides, and proteins to agricultural and biomedical sciences. *Journal of agricultural and food chemistry* **2004**, *52* (3), 385-406.
(9) Friedman, M.; Levin, C. E.; Noma, A. T.; Montague, W. C.; Zahnley, J. C. Comparison of tryptophan assays for food proteins. In *Progress in tryptophan and serotonin research*, De Gruyter, 2019; pp 119-124.
(10) Inglis, A. S. [5] Single hydrolysis method for all amino acids, including cysteine and tryptophan. In *Methods in Enzymology*, Vol. 91; Elsevier, 1983; pp 26-36.
(11) Yamada, H.; Moriya, H.; Tsugita, A. Development of an acid hydrolysis method with high recoveries of tryptophan and cysteine for microquantities of protein. *Analytical biochemistry* **1991**, *198* (1), 1-5.
(12) Dankoski, E. C.; Wightman, R. M. Monitoring serotonin signaling on a subsecond time scale. *Frontiers in integrative neuroscience* **2013**, *7*, 44.
(13) Hensley, A. L.; Colley, A. R.; Ross, A. E. Real-time detection of melatonin using fast-scan cyclic voltammetry. *Analytical chemistry* **2018**, *90* (14), 8642-8650.
(14) Murakami, Y.; Saito, K. Species and cell types difference in tryptophan metabolism. *International Journal of Tryptophan Research* **2013**, *6*, IJTR-S11558.
(15) Höglund, E.; Øverli, Ø.; Winberg, S. Tryptophan metabolic pathways and brain serotonergic activity: a comparative review. *Frontiers in endocrinology* **2019**, 158.
(16) Weese-Myers, M. E.; Ross, A. E. Characterization of electroactive amino acids with fast-scan cyclic voltammetry. *Journal of The Electrochemical Society* **2021**, *168* (12), 126524.
(17) Stafford, J. M.; Lee, C.-H.; Voigt, P.; Descostes, N.; Saldaña-Meyer, R.; Yu, J.-R.; Leroy, G.; Oksuz, O.; Chapman, J. R.; Suarez, F. Multiple modes of PRC2 inhibition elicit global chromatin alterations in H3K27M pediatric glioma. *Science advances* **2018**, *4* (10), eaau5935.
(18) Nguyen, N. T.; Wrona, M. Z.; Dryhurst, G. Electrochemical oxidation of tryptophan. *Journal of Electroanalytical Chemistry and Interfacial Electrochemistry* **1986**, *199* (1), 101-126. DOI: https://doi.org/10.1016/0022-0728(86)87045-0.
(19) Enache, T. A.; Oliveira‐Brett, A. M. Pathways of electrochemical oxidation of indolic compounds. *Electroanalysis* **2011**, *23* (6), 1337-1344.
(20) Calhoun, S. E.; Meunier, C. J.; Lee, C. A.; McCarty, G. S.; Sombers, L. A. Characterization of a multiple-scan-rate voltammetric waveform for real-time detection of met-enkephalin. *ACS Chemical Neuroscience* **2018**, *10* (4), 2022-2032.

(21) Schmidt, A. C.; Dunaway, L. E.; Roberts, J. G.; McCarty, G. S.; Sombers, L. A. Multiple scan rate voltammetry for selective quantification of real-time enkephalin dynamics. *Analytical chemistry* **2014**, *86* (15), 7806-7812.
(22) Takmakov, P.; Zachek, M. K.; Keithley, R. B.; Walsh, P. L.; Donley, C.; McCarty, G. S.; Wightman, R. M. Carbon Microelectrodes with a Renewable Surface. *Analytical Chemistry* **2010**, *82* (5), 2020-2028. DOI: 10.1021/ac902753x.
(23) Heien, M. L. A. V.; Phillips, P. E. M.; Stuber, G. D.; Seipel, A. T.; Wightman, R. M. Overoxidation of carbon-fiber microelectrodes enhances dopamine adsorption and increases sensitivity. *Analyst* **2003**, *128* (12), 1413-1419.
(24) Wipf, D. O.; Kristensen, E. W.; Deakin, M. R.; Wightman, R. M. Fast-scan cyclic voltammetry as a method to measure rapid heterogeneous electron-transfer kinetics. *Analytical Chemistry* **1988**, *60* (4), 306-310.
(25) Bard, A. J.; Faulkner, L. R.; White, H. S. *Electrochemical methods: fundamentals and applications*; John Wiley & Sons, 2022.
(26) Paras, C. D.; Kennedy, R. T. Amperometry and cyclic voltammetry of tyrosine and tryptophan‐containing oligopeptides at carbon fiber microelectrodes applied to single cell analysis. *Electroanalysis* **1997**, *9* (3), 203-208.
(27) Walther, D. J.; Peter, J.-U.; Bashammakh, S.; Hortnagl, H.; Voits, M.; Fink, H.; Bader, M. Synthesis of serotonin by a second tryptophan hydroxylase isoform. *Science* **2003**, *299* (5603), 76-76.
(28) Ottenhof, K. W.; Sild, M.; Lévesque, M. L.; Ruhé, H. G.; Booij, L. TPH2 polymorphisms across the spectrum of psychiatric morbidity: a systematic review and meta-analysis. *Neuroscience & Biobehavioral Reviews* **2018**, *92*, 29-42.
(29) Nemoto, T.; Horie, S.; Okuma, Y.; Nomura, Y.; Murayama, T. Possible involvement of amino acid transporters on S-nitroso-cysteine-induced inhibition of arachidonic acid release in PC12 cells. *Neuroscience letters* **2001**, *311* (2), 117-120.
(30) Nemoto, T.; Shimma, N.; Horie, S.; Saito, T.; Okuma, Y.; Nomura, Y.; Murayama, T. Involvement of the system L amino acid transporter on uptake of S-nitroso-l-cysteine, an endogenous S-nitrosothiol, in PC12 cells. *European journal of pharmacology* **2003**, *458* (1-2), 17-24.

For Table of Contents Only

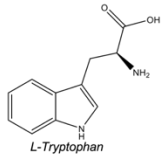

L-Tryptophan